Momentum-Resolved Lifetimes of Image-Potential States on Cu(100)

W. Berthold and U. Höfer
Fachbereich Physik und Zentrum für Materialwissenschaften, Philipps-Universität, D-35032 Marburg, Germany

P. Feulner
Physik-Department E20, Technische Universität München, D-85748 Garching, Germany

E. V. Chulkov, V. M. Silkin, and P. M. Echenique
Donostia International Physics Center (DIPC), Departamento de Física de Materiales and Centro Mixto CSIC-UPV/EHU, Universidad del Pais Vasco, 20018 San Sebastián, Basque Country, Spain
(Received 25 October 2001; published 18 January 2002)

The dependence of the inelastic lifetime of electrons in the image-potential states of Cu(100) on their momentum parallel to the surface has been studied experimentally by means of time- and angle-resolved two-photon photoemission and theoretically by evaluating the electron self-energy within the *GW* approximation. The pronounced decrease of the $n = 1$ lifetime from 40 fs at normal emission ($k_{\parallel} = 0$) to 20 fs for $k_{\parallel} = 0.33$ Å^{-1} cannot be accounted for by interband decay processes to bulk states. We show that *intraband* transitions within the image-state band give a contribution to this decrease comparable in magnitude with the interband channel.

DOI: 10.1103/PhysRevLett.88.056805 PACS numbers: 73.20.At, 71.45.Gm, 78.47.+p, 79.60.Bm

Electrons excited at a metal surface will in general be subject to fast decay by the exchange of both energy and momentum with the underlying three-dimensional electronic system of the bulk. Relaxation processes of this type are crucial for many important surface phenomena, such as electronically induced adsorbate reactions or electron transfer across interfaces [1–3]. For example, by using ultrafast techniques, time-resolved observation of nuclear motion is possible that provides information not only on the reaction time but also serves to explore the shape of the excited potential energy surface. However, this could be accomplished thus far only for one system, Cs/Cu(111), where the adsorbate resonance features a relatively long lifetime of tens of femtoseconds [4,5].

Image-potential states represent a promising model system for which a detailed understanding of the fundamental mechanisms of electron dynamics at surfaces can be achieved. In the normally unoccupied, hydrogenlike image states, the electrons are bound only in the perpendicular coordinate and exhibit free-electron-like dispersion parallel to the surface [6–8]. These simple and well-defined physical properties make realistic self-energy calculations of the decay rate feasible [9–11]. Recent theoretical work, that compares well with the results of direct time-domain investigations by two-photon photoemission (2PPE) [12,13], has elucidated the main factors that determine the coupling of image-potential states to the substrate and thus their lifetime for inelastic decay: the penetration of the image state wave function into the sp-gap of the metal, the presence of an evanescent tail of bulk states outside the crystal, and the reduced electronic screening in the transition region between vacuum and metal [14].

In this Letter, we focus on momentum-dependent investigations. We have studied the Cu(100) surface by time- and angle-resolved 2PPE and by many-body theory within the *GW* approximation. Although it has been suggested earlier that image-state electrons may decay by intraband transitions within the image-state band [9], little attention has been paid thus far to momentum-dependent relaxation processes. Our results show that intraband scattering does indeed contribute substantially to the decay rate at finite parallel momentum.

In our experiment we used the 60-fs pulses of the third harmonic of a Ti:sapphire oscillator to populate the image-potential states from metal states below the Fermi level. The photon energy was set to $\hbar\omega_a = 4.65$ eV, slightly below the work function of Cu(100), in order to excite the complete band system up to the vacuum energy and simultaneously avoid the strong background from one-photon photoemission. A part of the fundamental laser beam served as a probe by lifting a fraction of the excited electrons above the vacuum energy. The photoelectrons emitted from the sample were passed through a hemispherical analyzer with energy and momentum resolution of 22 meV and ± 0.015 Å^{-1}, respectively. Time resolution is obtained by recording the 2PPE signal as a function of the time delay between the pump and the probe pulses. The Cu(100) sample was prepared by standard sputtering and annealing procedures. Surface cleanliness and order was verified by x-ray photoemission spectroscopy, LEED, and by linewidth measurements with 2PPE [15]. The sample was kept in a UHV chamber with a base pressure of 6×10^{-11} mbar. It could be cooled to a temperature of 24 K by a liquid helium cryostat.

A general description of our theoretical methods has been given in Refs. [11,14]. Here, we only summarize items which are specific for this work. By applying the non-self-consistent *GW* approximation [16] and making

use of the translational symmetry in the plane parallel to the surface, the decay rate is calculated as (employing atomic units $\hbar = m = e = 1$)

$$\tau^{-1} = -2 \sum_{E_F \le E_f \le E_0} \int \frac{d^2\mathbf{q}_\parallel}{(2\pi)^2} \int dz \int dz' \, \phi_0^*(z)\phi_f(z)\,\mathrm{Im}W(z,z';\mathbf{q}_\parallel,E_0 - E_f)\phi_0(z')\phi_f^*(z')\,, \quad (1)$$

where $\mathrm{Im}W(z,z';\mathbf{q}_\parallel,E_0 - E_f)$ is the two-dimensional Fourier transform of the imaginary part of the screened Coulomb interaction (see [14] for details). $E_0 = E_{0z} + \mathbf{k}_\parallel^2/2m_0$ and $E_f = E_{fz} + (\mathbf{k}_\parallel + \mathbf{q}_\parallel)^2/2m_f$ are the energies of the initial and the final state, respectively; $\mathbf{q}_\parallel$ is the exchanged momentum. The wave functions $\phi(z)$ in the direction normal to the surface were obtained by solving the one-dimensional Schrödinger equation for a well-established model potential which accounts for the electronic structure of the surface by reproducing the experimentally observed upper and lower edge of the bulk projected band gap [17]. Because each of the two band edges disperses differently with parallel momentum, the image-state wave function was computed for every value of $\mathbf{k}_\parallel$ separately leading to wave functions that depend on parallel momentum.

Typical time- and momentum-resolved experimental data for the $n = 1$ state are displayed in Fig. 1. The exponential decay of the signal can be followed over several orders of magnitude from which the lifetimes are obtained independently of the underlying model to describe the 2PPE process. In this study we fitted the data by simple rate equations. We observe that the lifetimes decrease with increasing parallel momentum, e.g., the lifetime of $n = 1$ at the $\overline{\Gamma}$ point ($k_\parallel = 0$) is $\tau = 40$ fs while at $k_\parallel = 0.24$ Å^{-1} we find $\tau = 25$ fs. Also present in the signal is a weak shoulder showing up at delay times around 300 fs which exhibits a considerably longer lifetime of 120–130 fs. As will be discussed elsewhere, this shoulder is caused by image-state electrons primarily excited to the $n = 2$ state that are resonantly scattered to $n = 1$ [18]. Since the total signal arising from this channel amounts to less than 1% under the present experimental conditions, the deduced momentum-dependent decay rates are not affected by the detailed dynamics of this scattering process. The measured lifetimes did not depend on temperature between 24 and 300 K (see also Ref. [18]).

A plot of the measured decay rates $\Gamma = \hbar/\tau$ as a function of the kinetic energy of parallel motion $E_\parallel = \hbar^2\mathbf{k}_\parallel^2/2m_0$ (Fig. 2) reveals an approximately linear increase. The slopes are $d\Gamma/dE = 47$ meV/eV and 11 meV/eV for $n = 1$ and 2, respectively. For the $n = 1$

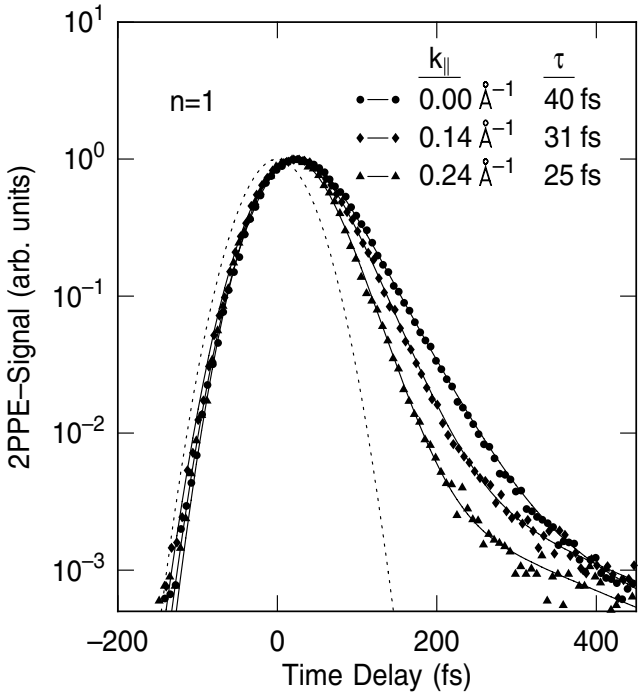

FIG. 1. $n = 1$ pump-probe traces for different values of parallel momentum (symbols) plotted on a logarithmic scale and fitted with exponentials (lines). Positive delay times indicate that the probe pulse arrives at the sample after the pump pulse. The dotted line is the computed pump-probe cross correlation, which denotes the experimental instrument function with a full width at half maximum of 90 fs.

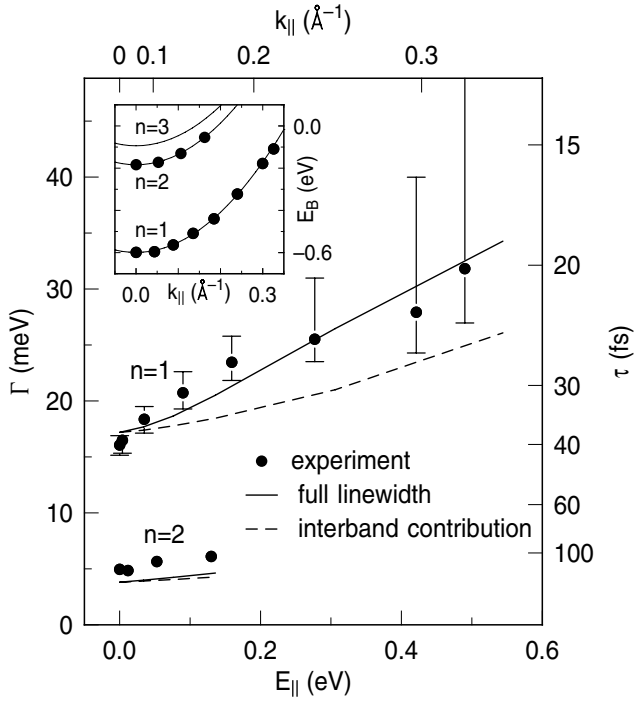

FIG. 2. Experimental (dots) and theoretical (solid lines) lifetimes and decay rates ($\Gamma = \hbar/\tau$, $\hbar = 658$ meV fs) of the first two image states $n = 1, 2$ as a function of excitation energy $E_\parallel$ above the respective band bottom. Computed decay rates without the contribution of intraband relaxation are shown as dashed lines. Inset: Measured dispersion of $n = 1, 2$ parallel to the surface.

state, the agreement between the results of our many-body calculations and the experiment is excellent. Both the decay rate at the $\overline{\Gamma}$ point and the increase of Γ with energy are satisfyingly reproduced. For $n = 2$ we get good quantitative agreement of the slope $d\Gamma/dE$, whereas the absolute magnitude of the experimental decay rate is slightly higher than predicted theoretically [11].

Two major decay channels have been considered for the calculation. First, an excited electron can be removed from the image-state band and escape into the metal. This process, in the following called *interband decay to the bulk,* is sketched in the inset of the lower part of Fig. 3. It is the only decay mechanism available at the band minimum ($k_\parallel = 0$). In agreement with our previous results [11,12], experiment and theory fit together nicely at this point of the surface Brillouin zone. However, interband decay to the bulk (dashed lines in Fig. 2) significantly underestimates the experimentally observed momentum dependence. The increase of the decay rate with parallel momentum is to a remarkably large extent (approximately 50%) determined by a second decay channel that is available to electrons with finite parallel momentum. In this process of *intraband scattering,* the electrons remain inside the image-state band but change their momentum and relax towards the band minimum. As sketched in the inset of the upper part of Fig. 3, this relaxation pathway is also mediated by the interaction with bulk electrons and leads to a corresponding excitation that takes up the loss of energy and momentum.

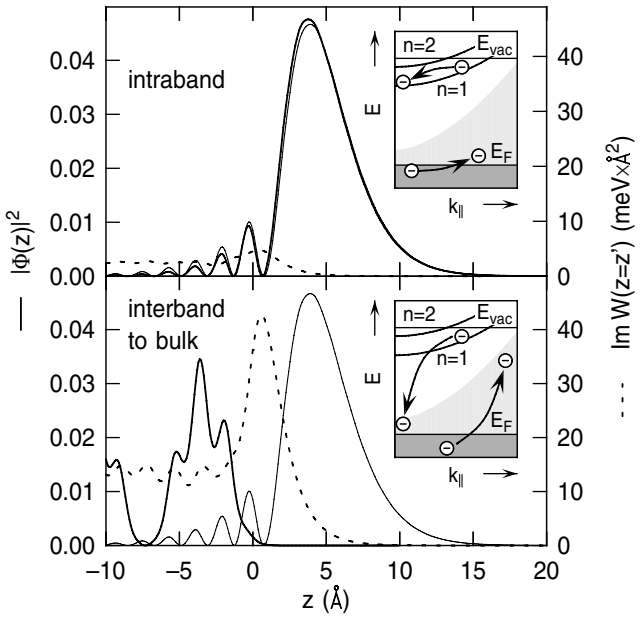

FIG. 3. Imaginary part of the screened Coulomb interaction $\mathrm{Im}W(z = z')$ (dashed line) and the final state probability density $|\phi_f|^2$ (thick solid line) computed for typical cases of the decay of an $n = 1$ image-state electron with probability density $|\phi_0|^2$ (thin solid line). Top: Intraband scattering. The energy exchange is $E_0 - E_f = 0.55$ eV. Bottom: Interband decay with energy exchange $E_0 - E_f = 3.5$ eV. Momentum exchange is $|\mathbf{q}_\parallel| = 0.38$ Å^{-1} in both cases. The insets illustrate the different decay processes.

A deeper understanding of the observed momentum dependence can be obtained from analyzing the different quantities that influence the decay rate Γ via Eq. (1). First, for small energy and momentum transfer in bulk metals the screened Coulomb interaction follows the general dependence $\mathrm{Im}W \propto (E_0 - E_f)/|\mathbf{q}_\parallel|$ [14]. Although near surfaces the momentum dependence becomes more complicated, the decay rate should increase with exchanged energy and decrease with exchanged momentum. Second, by neglecting the nonlocality of $\mathrm{Im}W$, i.e., by setting $z = z'$, it can be seen that Γ depends linearly on the wave function overlap $|\int dz\, \phi_0^*(z)\phi_f(z)|^2$ between the initial state and the final state. Finally, Γ increases with the density of final states as expressed by the summation in Eq. (1).

Based on these physics, the great importance of intraband scattering can be understood (compare Fig. 3). In the case of interband decay to the metal, the energy exchange is large, as is the screened interaction $\mathrm{Im}W \propto (E_0 - E_f)$, but the image state electron is mainly located outside the metal in the vacuum. As a result, there is only little spatial overlap between the wave functions of the initial image state and the final bulk state, limiting the decay due to this process. In the case of intraband decay, on the other hand, the energy exchange is small and, consequently, $\mathrm{Im}W$. But there is almost complete spatial overlap between the initial state and the final state, because both are image states with the same quantum number n though different $\mathbf{k}_\parallel$. This makes both decay channels comparable in magnitude.

For other systems the situation can be very different. The hole decay rate on the (111) noble metal surfaces, e.g., is almost completely determined by intraband scattering, because both the wave function overlap and $\mathrm{Im}W$ favor this decay channel [19]. Our results contrast electron dynamics on semiconductor surfaces, where phonon scattering plays a dominant role [20]. There, the existence of the band gap suppresses electronic decay, which would be otherwise orders of magnitude more effective than phononic mechanisms. Similarly, intraband decay of image-potential states was first observed in the presence of dielectric adlayers. These insulating films cause decoupling from the bulk electronic system, and adsorbate motion is believed to be mainly responsible for redistribution in momentum space [21,22].

Our calculations have shown that intraband scattering is an important mechanism for the decay of image-state electrons. As a consequence, part of the electrons, primarily excited with a finite parallel momentum, are expected to cascade down the two-dimensional parabolic band to the $\overline{\Gamma}$ point before they decay to bulk states. For a situation where the $n = 1$ band is homogeneously populated up to the vacuum level (pump photon energy $\hbar\omega_a = 4.65$ eV), theoretical modeling predicts that as much as 35% of the 2PPE signal at normal emission originates from secondary electrons. Since excitation by the pump pulse, decay to the bulk, and intraband cascading, all take place on a similar

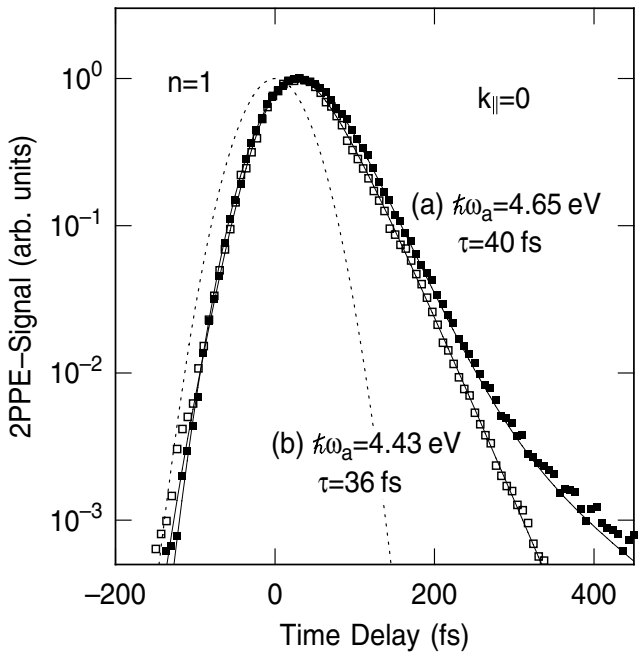

FIG. 4. $n = 1$ pump-probe traces at $k_{\|} = 0$ recorded under different excitation conditions: (a) The photon energy $\hbar\omega_a$ of the pump pulses is adjusted in order to excite the complete band up to the vacuum energy. (b) The photon energy $\hbar\omega_a$ is set to a smaller value where only $2/3$ of the band is excited. Thin lines indicate simulations of the cascade processes; the dashed line is the computed instrument function as in Fig. 1.

time scale of tens of femtoseconds, the delayed arrival of the secondary electrons at the $\overline{\Gamma}$ point does not manifest itself in a clearly visible separate decay rate in pump-probe traces such as those shown in Fig. 1.

Nevertheless, we could experimentally verify the prediction of cascade processes by performing 2PPE measurements with different pump photon energies $\hbar\omega_a$. If $\hbar\omega_a$ is reduced by $\sim$0.2 eV, then only 67% of the $n = 1$ band can be excited. Under this condition, the signal at the band minimum ($k_{\|} = 0$) exhibits a slightly but experimentally significantly shorter decay time of 36 fs instead of 40 fs (Fig. 4). We have simulated these cascade processes with a rate equation model based on our theoretical energy dependence of the relative strengths of intraband and interband decay. Both data sets can be reproduced accurately with only one free parameter that slightly adjusts the absolute decay rate. The present results show that—depending on the photon energy used for the pump pulses—2PPE experiments may overestimate the $n = 1$ lifetime at the $\overline{\Gamma}$ point by as much as 20% due to intraband scattering. In order to extract lifetimes experimentally, the generation of electron cascades should in general be avoided by using pump pulses close to the excitation threshold.

In summary, the inelastic lifetime associated with image-potential states on Cu(100) was observed to decrease appreciably as a function of parallel momentum of the electron. Besides the well-known interband relaxation to bulk states, intraband scattering within the parabolic surface bands was shown to play a remarkably strong role at finite parallel momentum. The resulting cascade processes and generation of secondary electrons should also be taken into account for accurate modeling of coherent and incoherent dynamics at zero momentum.

This work was funded by the Deutsche Forschungsgemeinschaft through SFB 338 and HO2295/3. Part of the equipment was provided by the Max-Planck-Institut für Quantenoptik in Garching. Support from the University of the Basque Country, the Basque Hezkuntza, Spanish MEC, and the Max Plank Research Award funds is also gratefully acknowledged.

[1] P. Feulner and D. Menzel, in *Laser Spectroscopy and Photochemistry on Metal Surfaces,* edited by H. L. Dai and W. Ho (World Scientific, Singapore, 1995), p. 627; W. Wurth and D. Menzel, Chem. Phys. **251**, 141 (2000).
[2] E. W. Plummer, Science **277**, 1447 (1997); M. Wolf and G. Ertl, Science **288**, 1352 (2000).
[3] A. G. Borisov *et al.,* Phys. Rev. Lett. **86**, 488 (2001).
[4] H. Petek, M. J. Weida, H. Nagano, and S. Ogawa, Science **288**, 1402 (2000).
[5] M. Bauer, S. Pawlik, and M. Aeschlimann, Phys. Rev. B **55**, 10 040 (1997); S. Ogawa, H. Nagano, and H. Petek, Phys. Rev. Lett. **82**, 1931 (1999).
[6] P. M. Echenique and J. B. Pendry, J. Phys. C **11**, 2065 (1978).
[7] Th. Fauster and W. Steinmann, in *Photonic Probes of Surfaces,* edited by P. Halevi (North-Holland, Amsterdam, 1995), pp. 347–411.
[8] R. M. Osgood, Jr. and X. Wang, Solid State Phys. **51**, 1 (1997).
[9] P. M. Echenique, F. Flores, and F. Sols, Phys. Rev. Lett. **55**, 2348 (1985).
[10] J. J. Deisz and A. G. Eguiluz, Phys. Rev. B **55**, 9195 (1997).
[11] E. V. Chulkov *et al.,* Phys. Rev. Lett. **80**, 4947 (1998).
[12] U. Höfer *et al.,* Science **277**, 1480 (1997); I. L. Shumay *et al.,* Phys. Rev. B **58**, 13 974 (1998).
[13] M. Wolf, E. Knoesel, and T. Hertel, Phys. Rev. B **54**, R5295 (1996); E. Knoesel, A. Hotzel, and M. Wolf, J. Electron Spectrosc. Relat. Phenom. **88–91**, 577 (1998).
[14] P. M. Echenique *et al.,* Chem. Phys. **251**, 1 (2000).
[15] Ch. Reuß *et al.,* Phys. Rev. Lett. **82**, 153 (1999).
[16] For a detailed discussion of the applicability of the non-self-consistent *GW* approximation, see, e.g., B. Holm and U. von Barth, Phys. Rev. B **57**, 2108 (1998); F. Bechstedt, K. Tenelsen, B. Adolph, and R. Del Sole, Phys. Rev. Lett. **78**, 1528 (1997).
[17] E. V. Chulkov, V. M. Silkin, and P. M. Echenique, Surf. Sci. **391**, L1217 (1997); **437**, 330 (1999).
[18] W. Berthold, J. Güdde, P. Feulner, and U. Höfer, Appl. Phys. B **73**, 865 (2001).
[19] J. Kliewer *et al.,* Science **288**, 1399 (2000).
[20] R. Haight, Surf. Sci. Rep. **21**, 275 (1995).
[21] C. M. Wong *et al.,* J. Phys. Chem. B **103**, 282 (1999).
[22] A. Hotzel, M. Wolf, and J. P. Gauyacq, J. Phys. Chem. B **104**, 8438 (2000).